NMR evidence of anisotropic Kondo liquid behavior in $CeIrIn_5$

A. C. Shockley,[1,*] K. R. Shirer,[2] J. Crocker,[2] A. P. Dioguardi,[2] C. H. Lin,[2] D. M. Nisson,[2]
N. apRoberts-Warren,[2] P. Klavins,[2] and N. J. Curro[2]
[1]*Laboratoire de Physique des Solides, Université Paris-Sud 11, UMR CNRS 8502, 91405 Orsay, France*
[2]*Department of Physics, University of California, Davis, California 95616, USA*
(Received 4 July 2014; published 5 August 2015)

We report detailed Knight-shift measurements of the two indium sites in the heavy-fermion compound $CeIrIn_5$ as a function of temperature and field orientation. We find that the Knight-shift anomaly is orientation dependent, with a crossover temperature T^* that varies by 50% as the field is rotated from (001) to (100). This result suggests that the hybridization between the Ce $4f$ states and the itinerant conduction electrons is anisotropic, a result that reflects its collective origin, and may lead to anisotropic Kondo liquid behavior and unconventional superconductivity.

DOI: 10.1103/PhysRevB.92.085108 PACS number(s): 75.30.Mb, 71.27.+a, 74.70.Tx, 76.60.Cq

I. INTRODUCTION

Heavy-electron materials exhibit a number of interesting correlated electron phenomena, including unusual broken-symmetry ground states, quantum criticality, and non-Fermi-liquid behavior, which arise from the interactions between a lattice of nearly localized $4f$ electrons and itinerant conduction electron states [1,2]. When the $4f$ states are weakly hybridized with the itinerant states, the materials tend to exhibit long-range antiferromagnetism mediated by Ruderman-Kittel-Kasuya-Yosida (RKKY) interactions; in the opposite limit the long-range order disappears, the resulting itinerant quasiparticles have enhanced effective masses, and the system typically is unstable towards unconventional superconductivity [3–5]. The emergence of a heavy-fermion fluid in close proximity to an antiferromagnetic instability of localized moments remains an active area of experimental and theoretical research. Several Ce-based compounds happen to exhibit a level of hybridization that places them close to the quantum critical (QC) boundary between long-range antiferromagnetism and superconductivity. As a result small perturbations induced by doping or pressure can result in dramatic changes to the ground-state properties [6,7]. These compounds offer an ideal testing ground to investigate the interplay between the hybridization and the emergent states of the strongly correlated system.

$CeIrIn_5$ is an excellent example of a system close to a QC boundary; while it is superconducting below 0.4 K, the normal state exhibits antiferromagnetic fluctuations and non-Fermi-liquid behavior [8,9]. Thus this compound can provide vital information about the emergence of the coherent heavy-fermion fluid near a QC boundary. Dynamical mean field theory (DMFT) calculations indicate that $CeIrIn_5$ undergoes a crossover from localized to itinerant electron behavior with decreasing temperature, accompanied by changes to the Fermi surface [10,11]. Experimental evidence is provided by resistivity, specific heat, and nuclear magnetic resonance (NMR) Knight-shift measurements which are well described by a two-fluid picture of heavy-fermion behavior [12]. Recent calculations have shown that this hybridization-driven crossover is strongly anisotropic in this material [13]. Here we provide direct experimental evidence for such hybridization anisotropy, which may play a key role in stabilizing the unconventional superconductivity in this family of heavy fermions. The DMFT calculations indicate that since the local $4f$ states are anisotropic, the hybridization is dominated by the orbital overlap between the Ce $4f$ and the out-of-plane In(2) electron orbitals (see Fig. 1). This hybridization should be manifest in the spin susceptibility χ_{cf}, describing the correlations between the itinerant and local moment electron spins. This quantity can be directly probed via Knight-shift experiments [14,15]. We have conducted detailed angular-dependent studies of the In(1) and In(2) Knight shifts and have found that χ_{cf} indeed depends on the orientation of the applied magnetic field with respect to the crystal axes. The temperature dependence of this correlation function is determined by the Kondo lattice coherence temperature T^*, which we find to be largest along the Ce-In(2) bond axis.

II. KNIGHT-SHIFT MEASUREMENTS

High-quality single crystals of $CeIrIn_5$ were synthesized using the standard flux method described in Ref. [16]. Characterization with powder x-ray diffraction showed the samples were pure with a small amount of In flux [17]. A large single crystal with the dimensions $3 \times 3 \times 1$ mm was chosen for the NMR studies, which were performed in an Oxford high-homogeneity magnet at a fixed field of 11.7 T. All spectra were obtained using a standard Hahn echo pulse sequence [18]. The orientation of the sample was controlled by a single-axis goniometer, and the sample was mounted such that the applied field was directed at an angle θ from (001), in the plane spanned by (100) and (001), as shown in Fig. 1(a). For each angle, a full spectrum including several different satellite transitions of ^{115}In($I = 9/2$) was obtained using an automated tuning system integrated with the NMR spectrometer. The quadrupolar nature of this isotope enabled us to extract the orientation of the field, and hence the Knight shift, as described in detail in the Appendix. There are four In(2) sites per unit cell, and when $\theta > 0$, these four sites split into two inequivalent sites depending on whether the field is parallel or perpendicular to the face of the unit cell [see

*Previously at Department of Physics, University of California, Davis, California 95616, USA; acshoc@gmail.com

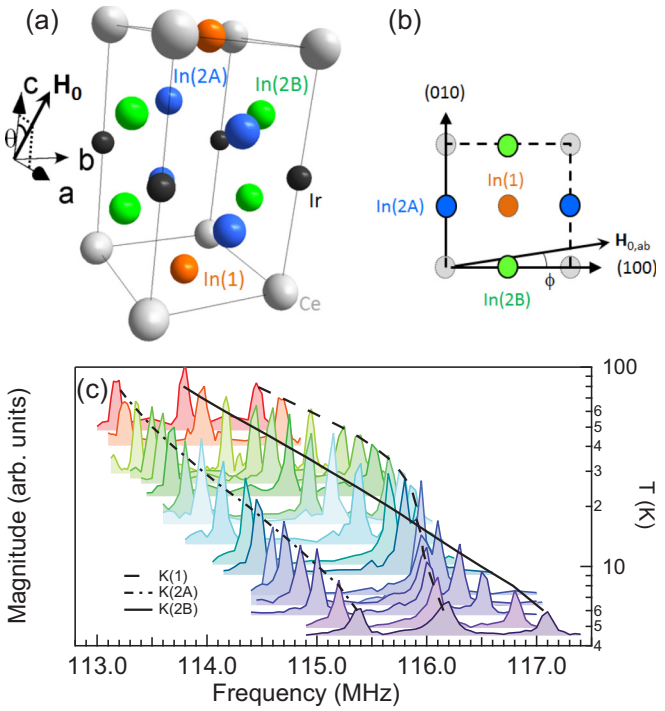

FIG. 1. (Color online) (a) Unit cell indicating the three indium sites and the field orientation. (b) Projection of the unit cell in the ab plane. (c) A representative frequency-swept spectrum of $CeIrIn_5$ at 11.7 T for $\theta = 44^\circ$ and temperatures from 6 to 80 K; the magnitude is normalized by temperature. The temperature-dependent Knight shifts for the In(1), In(2A), and In(2B) sites are scaled over the raw spectral data.

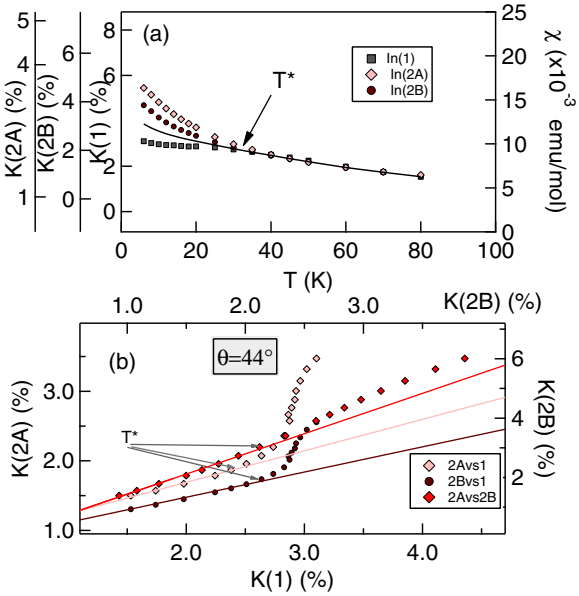

FIG. 2. (Color online) (a) Knight shift at $\theta = 44^\circ$ (solid points) and bulk susceptibility $\chi(T) = \chi_c \cos^2(\theta) + \chi_a \sin^2(\theta)$ vs temperature (solid line). (b) $K(2A)$ and $K(2B)$ vs $K(1)$ and $K(2A)$ vs $K(2B)$ with temperature implicit. Solid lines are fits to the high temperature ($T > T^*$). T^* is the temperature below which the linear relationship between these quantities breaks down.

Fig. 1(b)]. We refer to these two In(2) sites as In(2A) and In(2B). Characteristic spectra of the In(1), In(2A), and In(2B) sites are shown in Fig. 1(c) for $\theta = 44^\circ$ at several different temperatures. Each of the three sites clearly exhibits different temperature-dependent behaviors. Detailed spectra were also measured at various rotation angles in order to observe any anisotropy in the temperature dependence.

For a spin-1/2 nucleus, the resonance frequency is given by $\omega = \gamma H_0[1 + K(\theta,\phi)]$, where γ is the gyromagnetic ratio, H_0 is the magnetic field, and $K(\theta,\phi) = \mathbf{H}_0 \cdot \mathbb{K} \cdot \mathbf{H_0}/H_0^2$. Here $\mathbb{K}$ is the Knight-shift tensor, with principal axes lying along the unit-cell directions. In general, the Knight shift arises because of the hyperfine coupling between the nuclear and electron spins of the material, which gives rise to an effective hyperfine field at the nuclear site in addition to the external field, thus shifting the resonance frequency. Hyperfine couplings can arise from on-site Fermi contact interactions, as well as via transferred couplings to electron spins located on neighboring atoms. The exact values of these couplings depend on details of the electronic structure of the material, are different for each site, and are generally difficult to compute. However, it is useful to consider an effective hyperfine interaction that is appropriate for heavy-fermion materials: $\mathcal{H}_{\rm hyp} = \hat{\mathbf{I}} \cdot (\mathbb{A} \cdot \mathbf{S}_c + \mathbb{B} \cdot \mathbf{S}_f)$, where $\mathbb{A}$ and $\mathbb{B}$ are temperature-independent hyperfine coupling tensors to the conduction electron and local moment spins, $\mathbf{S}_c$ and $\mathbf{S}_f$ [14]. $\hat{\mathbf{I}}$ is the nuclear spin on the ligand site, in this case either In(1), In(2A), or In(2B). In the paramagnetic state, the spins are polarized by the external field, and the Knight shift is given by $\mathbb{K} = \mathbb{K}_0 + \mathbb{A} \cdot \chi_{cc} + (\mathbb{A} + \mathbb{B}) \cdot \chi_{cf} + \mathbb{B} \cdot \chi_{ff}$, where $\chi_{ij} = \langle S_i S_j \rangle$ are the components of the total susceptibility $\chi = \chi_{cc} + 2\chi_{cf} + \chi_{ff}$, and $\mathbb{K}_0$ is the temperature-independent orbital shift tensor. For sufficiently large temperatures χ_{ff} is the dominant contribution; thus $\mathbb{K} \approx \mathbb{K}_0 + \mathbb{B} \cdot \chi$. As a result, K_α is linearly proportional to χ_α, where $\alpha = (a,b,c)$ are the principal directions of the tensor. Furthermore, since the shift of each site is proportional to χ, each shift is also proportional to the shifts of the other sites, as shown in detail in the Appendix. This linear dependence is evident in Fig. 2 for $T > T^*$.

Below the coherence temperature T^*, the conduction and local moment spin degrees of freedom become entangled, and χ_{cf} grows in magnitude relative to χ_{ff}. As a result, K_α is no longer proportional to χ_α, as seen in Fig. 2. T^* is a material-dependent crossover temperature that depends on the hybridization and intersite couplings between the S_f spins in the Kondo lattice [10,12,19,20]. T^* can be measured experimentally via independent measurements of K_α and χ_α: when K_α is plotted versus χ_α with temperature as an implicit variable, the linear relationship breaks down at T^*, as observed in Fig. 2 at $\theta = 44^\circ$. Several other pairs of shifts and angles are shown in Fig. 3, and in each case there is a clear break in this linear relationship at low temperatures.

In order to discern the influence of hybridization anisotropy, it is important to measure T^* as a function of angle. Our previous studies of the In(1) site in $CeIrIn_5$ indicated that $T^* \sim 40$ K and did not appear to vary significantly with field orientation or magnitude [15,21]. However, the precision of the T^* measurement is limited for the In(1) site because the coupling constants $A_a = B_a$ in the plane. Therefore the

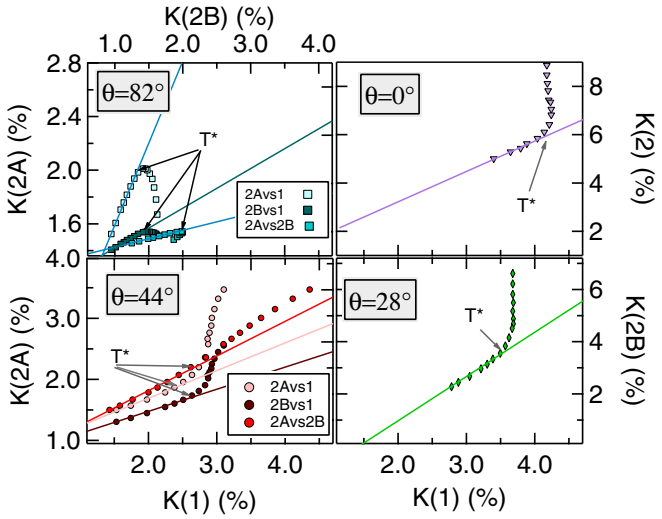

FIG. 3. (Color online) Clockwise from the top right panel: $K(2)]K(2A) = K(2B) = K(2)$ for this orientation] vs $K(1)$ for $\theta = 0^\circ$ (purple inverse triangles), $K(2B)$ vs $K(1)$ for $\theta = 28^\circ$ (green diamonds), $K(2A)$ and $K(2B)$ vs $K(1)$ and $K(2A)$ vs $K(2B)$ for $\theta = 44^\circ$ (pink, dark red, and red circles, respectively), and $K(2A)$ and $K(2B)$ vs $K(1)$ and $K(2A)$ vs $K(2B)$ for $\theta = 82^\circ$ (light blue, dark blue, and blue squares, respectively). Solid lines are fits to the high-temperature portion as described in the text. T^* is indicated by the gray arrows.

magnitude of the Knight-shift anomaly gradually decreases with angle and vanishes for $\mathbf{H}_0 \parallel (100)$. This problem can be circumvented by measuring the Knight shifts of both of the In(2) sites and the In(1) site. This approach is superior because all of the Knight-shift measurements can be acquired simultaneously at the same crystalline orientation without the need for separate measurements of χ [21]. The behavior below T^* is governed by the temperature dependence of the correlation function $\chi_{cf}(T)$. As the conduction electron and local moments become entangled, this quantity grows in magnitude and can be extracted from the Knight shift below T^*. To do so, we fit the high-temperature data ($T > T^*$)

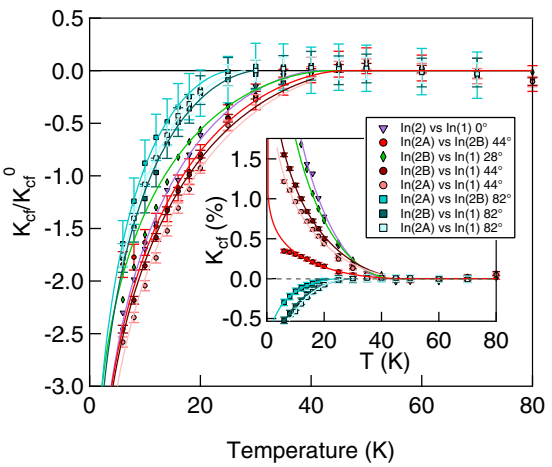

FIG. 4. (Color online) K_{cf}/K_{cf}^0 vs T for various angles (colors and symbols are defined as in Fig. 2). The solid lines are fits as described in the text. The inset shows K_{cf} vs T.

for each pair (K_1, K_2) of Knight shifts to $K_1 = a + bK_2$ and then plot $K_{cf}(\theta,T) = K_1(T,\theta) - a - bK_2(T,\theta)$ versus temperature in the inset of Fig. 4. As shown in the Appendix, this quantity is proportional to $\chi_{cf}(\theta,T)$ and becomes nonzero below T^*. The constants a and b depend on the ratios of hyperfine couplings of the various pairs of sites and are unimportant for our analysis [21]. We have confirmed that these constants are consistent for three different data sets.

III. ANISOTROPY

As seen in Fig. 4, K_{cf} vanishes above T^* but grows in magnitude with decreasing temperature below this temperature. These data clearly indicate that the onset temperature T^* depends on the angle θ. This angular variation is model independent and can be discerned in the plots of K_i versus K_j in Figs. 2 and 3. For concreteness we fit the temperature dependence of K_{cf} to the two-fluid expression [22],

$$K_{cf}(T) = K_{cf}^0(1 - T/T^*)^{3/2}[1 + \ln(T^*/T)], \qquad (1)$$

and plot K_{cf}^0 and T^* versus angle θ in Figs. 5(a) and 5(b). K_{cf}^0 is proportional to a complex ratio of the hyperfine couplings and anisotropic g factors of the material, and the angular dependence of this quantity seen in Fig. 5(a) reflects the anisotropies of these couplings. The main panel of Fig. 4 shows $K_{cf}(T)$ normalized by K_{cf}^0, which removes any anisotropies introduced by the hyperfine couplings and g factors. The onset temperature of the anomaly T^* varies with angle. Here T^* is unrelated to the hyperfine couplings and reflects intrinsic properties of the electronic degrees of freedom of the Kondo lattice. As seen in Figs. 4 and 5(b), as the field angle rotates from the (001) direction, T^* increases from 40 to nearly 50 K at 44° and then reaches a minimum of 26 K for the (100) direction. In order to parameterize

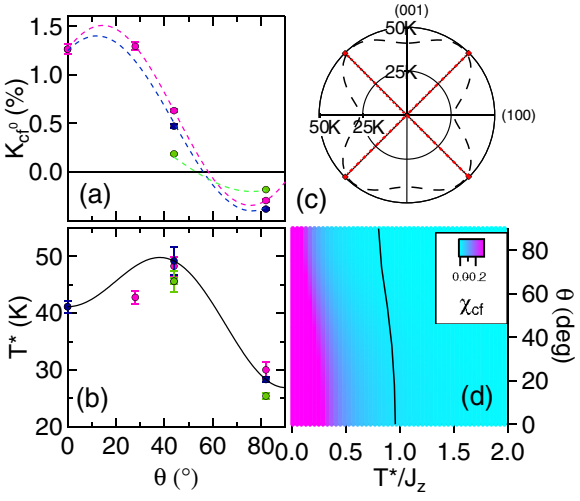

FIG. 5. (Color online) (a) K_{cf}^0 and (b) T^* vs angle as determined from the fits shown in Fig. 4, as determined by plotting $K(2B)$ vs $K(1)$ (pink), $K(2A)$ vs $K(1)$ (blue), and $K(2A)$ vs $K(2B)$ (green). Dashed lines are guides to the eye, and the solid line in (b) is a fit as described in the text. (c) $T^*(\theta)$ shown as a polar plot, relative to the (001) (vertical) and (001) (horizontal) directions. The dotted red lines indicate the Ce-In(2) directions. (d) $\chi_{cf}(T,\theta)$ and T^*/J_z (solid line) vs θ for the two-spin model discussed in the text.

this anisotropy, we fit this angular dependence to the form $T^*(\theta) = T_0^* + T_2^* \cos(2\theta) + T_4^* \cos(4\theta)$, which qualitatively reproduces the hybridization function calculated in Ref. [13]. We find $T_0^* = 42(2)$ K, $T_2^* = -7(2)$ K, and $T_4^* = 7(2)$ K, shown in Fig. 5(c). These results reveal that the heavy-electron fluid, which emerges from the collective hybridization of the lattice of $4f$ sites with the conduction electrons, is anisotropic in this material. This result suggests that the hybridization is not isotropic and has fourfold symmetry.

A. Hybridization

A recent analysis of data in a broad range of heavy-fermion materials indicated that T^* is proportional to the intersite RKKY exchange interaction, which itself is proportional to J^2, where the Kondo coupling J is a function of the hybridization [12]. Therefore anisotropy in the hybridization should be reflected in the experimentally measured quantity, T^*. In order to discern how an anisotropic hybridization can give rise to anisotropy in the susceptibility χ_{cf}, it is instructive to consider a generalization of the two-spin model introduced in Ref. [15]. We consider an anisotropic coupling between two free spins, $\mathbf{S}_c$ and $\mathbf{S}_f$: $\mathcal{H} = J_\perp(S_c^x S_f^x + S_c^y S_f^y) + J_z S_c^z S_f^z$, where $J_{z,\perp}$ is the coupling between the spins derived from the anisotropic hybridization parallel (perpendicular) to the z axis. This model is the single-site limit of the periodic Anderson model in the limit of large on-site repulsion U relative to the hybridization V, such that $J_\alpha = 4V_\alpha^2/U$ [20]. In this case, the susceptibilities χ_{cc}, χ_{cf}, and χ_{ff} are exactly solvable. For the isotropic case $J_\perp = J_z$, χ_{ij} are all isotropic and scale as T/T^*, where $T^* = J_z/k_B$. When $J_\perp \neq J_z$, these susceptibilities become anisotropic tensors, such that the susceptibility becomes angle dependent: $\chi_{cf}(T,\theta) = \chi_{cf}^z(T)\cos^2(\theta) + \chi_{cf}^\perp(T)\sin^2(\theta)$, shown in Fig. 5(d) for the case $J_\perp = 0.2J_z$. We fit this quantity to Eq. (1) for several values of θ, and the solid line in Fig. 5(d) shows the fitted values of $T^*(\theta)$. Clearly, T^* is anisotropic, although this model is not sophisticated enough to capture the fourfold variation observed in Fig. 5(b). A model including multiple sites would represent the full lattice better and would be more likely to resemble the experimental measures.

B. Crystalline electric field

An alternative interpretation of Knight-shift anomalies is that the hyperfine coupling constants depend on the particular crystalline electric field (CEF) doublets [23,24]. The strong spin-orbit coupling combined with CEF interactions at the Ce ions gives rise to a temperature-dependent anisotropic g factor. The Ce^{3+} ions in this material experience a CEF that splits the $J = 5/2$ ground-state multiplet into three doublets, with excited states energies $\Delta_1 = 6.7$ meV and $\Delta_2 = 29$ meV above the ground state [25,26]. In order to explore the possible role of the CEF in the anisotropy we observe in K_{cf}, we have computed K_{cf}^{CEF} and χ^{CEF} as a function of field orientation using the hyperfine coupling model discussed in Refs. [21,23,24]. In this scenario, the hyperfine coupling between the In(1) site and the Ce spin depends on the particular CEF doublet; thus when the temperature $T \lesssim \Delta_1/3k_B$, the thermal population of the excited states is significantly reduced, and the effective hyperfine field changes. As a result, the Knight shift differs from the susceptibility below the anomaly temperature $T_{\mathrm{CEF}}^* \sim \Delta_1/k_B$. Here we computed $\chi_{c,ab}^{\mathrm{CEF}}$ and $K_{c,ab}^{\mathrm{CEF}}$ using the same CEF parameters and hyperfine couplings as in Ref. [21] in a field of 11.7 T. These quantities are shown in Fig. 6. Note that these calculations do not accurately capture the behavior of the real material because this model neglects the role of hybridization of the Ce $4f$ states. Nevertheless, there is a clear anisotropy in the magnitudes of both K^{CEF} and χ^{CEF}, which reflects the anisotropy of the g factor of the Ce. We have also assumed isotropic hyperfine couplings in this calculation, but relaxing this assumption would simply modify the relative scale factors of the Knight shifts shown in Fig. 6.

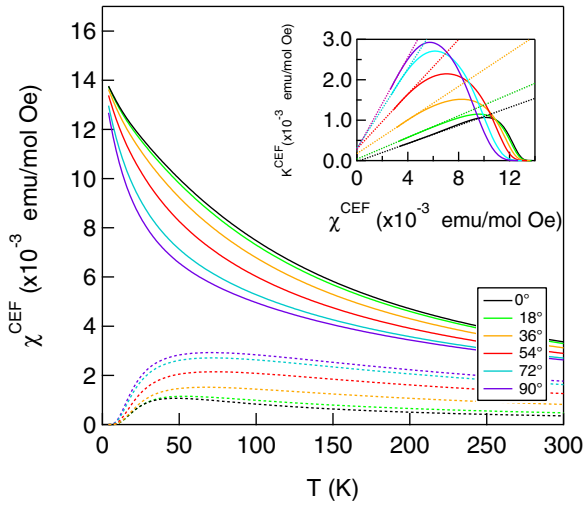

FIG. 6. (Color online) Susceptibility χ^{CEF} (solid lines) and Knight shifts K^{CEF} (dotted lines) vs temperature calculated in the CEF model for various field orientations, as described in the text. The inset shows K^{CEF} vs χ^{CEF} (solid lines) for the same orientations. Dashed lines are fits to the high-temperature data points.

We then fit the high-temperature portion ($T > 100$ K) of $K^{\mathrm{CEF}}(\theta)$ versus $\chi^{\mathrm{CEF}}(\theta)$ for various values of θ and plotted $K_{cf}^{\mathrm{CEF}}(\theta) = K^{\mathrm{CEF}}(\theta) - a - b\chi^{\mathrm{CEF}}(\theta)$, shown in Fig. 7(a). $\chi^{\mathrm{CEF}}(\theta)$ grows in magnitude below $T_{\mathrm{CEF}}^* \approx 55$ K $\sim 0.7\Delta_1$ and varies strongly with θ. For concreteness, we fit $K_{cf}^{\mathrm{CEF}}(\theta)$ to Eq. (1) to extract T_{CEF}^*, shown in Fig. 7(b). However, the fits, shown for $\theta = 0°$ and $90°$ as dotted lines in Fig. 7(a), are poor and do not capture well the detailed temperature dependence of the theoretical CEF curves. The fitted T^* increases from 64 to 120 K and then decreases down to 98 K as the field varies from the c axis to the ab plane. Figure 7(c) shows $K_{cf}^{\mathrm{CEF}}(\theta)$ normalized by K_{cf}^0 in order to remove the anisotropy of the g factor. Although the angular dependence of T^* extracted from these fits qualitatively reproduces the experimental observations, the temperature dependence of K_{cf}^{CEF} does not match well with the experimental data shown in Fig. 4. From these data alone, it is not possible to rule out this model, although previous work indicates that the field dependence of the Knight-shift anomaly is not captured by the CEF model [21]. It is possible that both CEF and hybridization effects could be playing a role in determining the anisotropic behavior we observe.

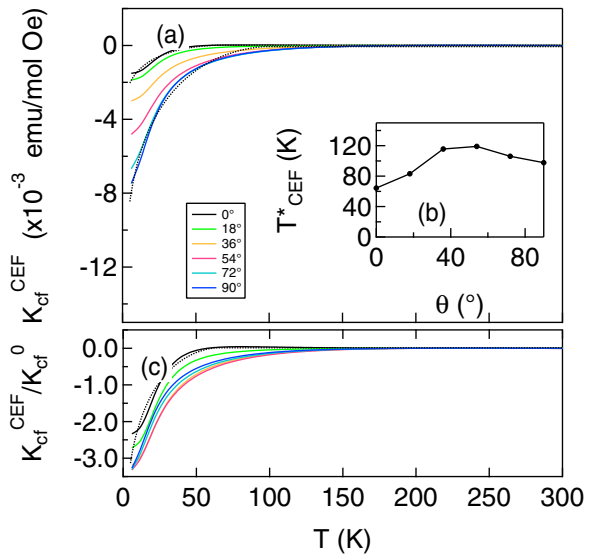

FIG. 7. (Color online) (a) K_{cf}^{CEF} vs T for several different field orientations (see legend in Fig. 6) using the fits to the high-temperature K^{CEF} vs χ^{CEF} relationship. (b) T^{*}_{CEF} extracted by fitting the theoretical K_{cf}^{CEF} results to Eq. (1) in the main text as a function of angle. (c) $K_{cf}^{\mathrm{CEF}}/K_{cf}^{0}$ vs T for various angles. The dotted line is a fit to Eq. (1) in the main text.

IV. DISCUSSION

An anisotropic coherence temperature has important implications in the context of the two-fluid model and can explain various observations. For example, in compounds such as $CeCoIn_5$ and $CeCu_2Si_2$, evidence suggests that the temperature onset of the Knight-shift anomaly differed when the field was parallel or perpendicular to the tetragonal c axis [14]. Our experiments on $CeIrIn_5$ suggest that hybridization anisotropy may also be present in these materials and call for further measurements. Anisotropy may also explain the variations in T^* measured by different experimental techniques such as NMR, resistivity, specific heat, or Hall measurements [12]. If there is a magnetic field present to break the symmetry, then experiments that couple to the susceptibility will reveal this anisotropy. On the other hand, for measurements in the absence of a field, such as resistivity or specific heat, the heavy-electron fluid will have an isotropic response with a slightly different temperature scaling. For example, in the isotropic case of the two-spin model discussed above, both the susceptibility and the specific heat scale as T/T^*, where $T^* = J_z/k_B = J_\perp/k_B$. However, when $J_\perp \neq J_z$ the susceptibility scales as $T/T^*(\theta)$, and the specific heat scales as T/T_C^*, where T_C^* is isotropic. In this case, both $T^*(\theta)$ and T_C^* are more complicated functions of J_z and $J_\perp$.

The anisotropy we observe in the static susceptibility will also be reflected in the dynamic susceptibility of the Kondo liquid, which may play a role in the emergence of superconductivity in this material. Anisotropic spin fluctuations have been shown to give rise to d-wave superconductivity and enhance T_c in for two-dimensional fluctuations [27]. Superconductivity appears to be fairly common in certain heavy-fermion families, such as the $CeMIn_5$ series, but not in other Ce-based heavy-fermion families. Our observations suggest the reason for the stability of superconductivity in the $CeMIn_5$ series may arise from the particular orbital overlap between the In(2) and the Ce sites in this structure, giving rise to the anisotropy in T^* we observe experimentally.

In summary, we have found evidence that the coherence temperature T^* as measured by the Knight shift is anisotropic in $CeIrIn_5$, reflecting an anisotropic collective hybridization in the Kondo lattice among multiple sites. Our results demonstrate that the NMR Knight shift is a vital new tool to explore and quantify this anisotropy and suggests that the In(2) sites in this compound play a key role in the development of the heavy-electron fluid. Detailed calculations, for example, quantum Monte Carlo simulations, should be carried out in order to test the effects of anisotropic hybridization and discern whether the fourfold symmetry we observe arises from collective hybridization among multiple sites.

ACKNOWLEDGMENTS

We thank Y.-F. Yang, D. Pines, M. Jiang, and R. Scalettar for enlightening discussions. A.C.S. would also like to thank F. Bert, I. Mukhamedshin, and P. Mendels. Work at UC Davis was supported by the NSF under Grant No. DMR-1005393.

APPENDIX

1. Spectrum analysis

Each spectrum, covering up to a range of 40 MHz, contains 9 In(1) transitions plus up to 18 In(2) transitions, depending on the orientation of the field with respect to the crystal. The resonance frequencies are determined by the NMR Hamiltonian: $\mathcal{H}_n = \gamma\hbar\hat{\mathbf{I}}\cdot(\mathbb{I}+\mathbb{K})\cdot\mathbf{H}_0 + \mathcal{H}_Q$, where $\mathbb{K}$ is the Knight-shift tensor, γ is the gyromagnetic ratio, $\mathbf{H}_0$ is the external applied field, and $\mathcal{H}_Q$ is the quadrupolar Hamiltonian. The latter is given by

$$\mathcal{H}_Q = \frac{\hbar}{6}\left[\omega_{zz}\left(3\hat{I}_z^2 - \hat{I}^2\right) + (\omega_{xx}-\omega_{yy})\left(\hat{I}_x^2 - \hat{I}_y^2\right)\right], \quad \text{(A1)}$$

where $(\omega_{xx},\omega_{yy},\omega_{zz})$ are the eigenvalues of the electric field gradient (EFG) tensor, with eigenvectors directed along the x,y,z directions. For the In(1) site, $\omega_{zz} = 6.07$ MHz along (001), and $\omega_{xx} = \omega_{yy} = -3.04$ MHz along (100) and (010). For In(2) $\omega_{zz} = 18.17$ MHz along (100), $\omega_{xx} = -13.26$ MHz along (010), and $\omega_{yy} = -4.91$ MHz along (001). $\mathcal{H}_n$ was diagonalized numerically, and the resonance frequencies were fit to the spectral data with the shift $K_{\alpha\alpha}$, the polar angle θ, and the azimuthal angle ϕ left as variable parameters. The In(1) site has axial symmetry; therefore there are nine equally spaced satellite transitions whose frequencies only depend on θ. For each orientation of the crystal, we fit the positions of the In(1) peaks in order to extract the angle θ. The azimuthal angle ϕ describes the orientation of $\mathbf{H}_0$ relative to (100). By analyzing the satellites of In(2) we found $\phi = 0^\circ \pm 2^\circ$ for each rotation of the goniometer.

2. Relationship between shifts of different sites

The hyperfine interaction is given by $\mathcal{H}_{\mathrm{hf}} = \hat{\mathbf{I}}\cdot[A\mathbf{S}_c + B\mathbf{S}_f]$, where A and B are the hyperfine couplings to the itinerant electron spins $\mathbf{S}_c$ and to the local moment spins $\mathbf{S}_f$.

In this case the Knight shift of each site is given by

$$K_i = K_i^0 + A_i\chi_{cc} + (A_i + B_i)\chi_{cf} + B_i\chi_{ff}, \quad \text{(A2)}$$

where i corresponds to In(1), In(2A), or In(2B); K_i^0 is a temperature independent orbital term; and the components of the susceptibility are given by $\chi_{\alpha\beta}$. The bulk susceptibility is $\chi = \chi_{cc} + 2\chi_{cf} + \chi_{ff}$. For $T > T^*$, χ_{cf} and χ_{cc} can be neglected; therefore $K_i = K_i^0 + B_i\chi$. In this case K_i is also linearly proportional to K_j: $K_i = a + bK_j$, where

$$a = K_i^0 - (B_i/B_j)K_j^0, \quad \text{(A3)}$$

$$b = B_i/B_j. \quad \text{(A4)}$$

These relationships enables us to extract χ_{cf} using just two pairs of Knight shifts without the need for independent measurements of χ. Using Eqs. (A2) and (A4), we find

$$\begin{aligned} K_{cf}(T) &= K_i(T) - a - bK_j(T) \\ &= \left(A_i - \frac{B_i}{B_j}A_j\right)[\chi_{cf}(T) + \chi_{cc}(T)]. \end{aligned} \quad \text{(A5)}$$

Since the hyperfine couplings are temperature independent and χ_{cc} can be neglected, this quantity is proportional to χ_{cf} and becomes nonzero below T^*.

[1] S. Doniach, Physica B+C **91**, 231 (1977).
[2] A. C. Hewson, *The Kondo Problem to Heavy Fermions* (Cambridge University Press, Cambridge, 1997).
[3] Z. Fisk, D. W. Hess, C. J. Pethick, D. Pines, J. L. Smith, J. D. Thompson, and J. O. Willis, Science **239**, 33 (1988).
[4] P. Coleman, C. Pepin, Q. M. Si, and R. Ramazashvili, J. Phys.: Condens. Matter **13**, R723 (2001).
[5] P. Coleman and A. J. Schofield, Nature (London) **433**, 226 (2005).
[6] T. Park, F. Ronning, H. Q. Yuan, M. B. Salamon, R. Movshovich, J. L. Sarrao, and J. D. Thompson, Nature (London) **440**, 65 (2006).
[7] S. Seo, X. Lu, J.-X. Zhu, R. R. Urbano, N. Curro, E. D. Bauer, V. A. Sidorov, L. D. Pham, T. Park, Z. Fisk, and J. D. Thompson, Nat. Phys. **10**, 120 (2014).
[8] C. Petrovic, R. Movshovich, M. Jaime, P. G. Pagliuso, M. F. Hundley, J. L. Sarrao, Z. Fisk, and J. D. Thompson, Europhys. Lett. **53**, 354 (2001).
[9] G.-q. Zheng, K. Tanabe, T. Mito, S. Kawasaki, Y. Kitaoka, D. Aoki, Y. Haga, and Y. Onuki, Phys. Rev. Lett. **86**, 4664 (2001).
[10] J. Shim, K. Haule, and G. Kotliar, Science **318**, 1615 (2007).
[11] H. C. Choi, B. I. Min, J. H. Shim, K. Haule, and G. Kotliar, Phys. Rev. Lett. **108**, 016402 (2012).
[12] Y.-F. Yang, Z. Fisk, H.-O. Lee, J. D. Thompson, and D. Pines, Nature (London) **454**, 611 (2008).
[13] K. Haule, C.-H. Yee, and K. Kim, Phys. Rev. B **81**, 195107 (2010).
[14] N. J. Curro, B.-L. Young, J. Schmalian, and D. Pines, Phys. Rev. B **70**, 235117 (2004).
[15] K. R. Shirer, A. C. Shockley, A. P. Dioguardi, J. Crocker, C. H. Lin, N. apRoberts-Warren, D. M. Nisson, P. Klavins, J. C. Cooley, Y.-f. Yang, and N. J. Curro, Proc. Natl. Acad. Sci. USA **109**, E3067 (2012).
[16] E. Moshopoulou, Z. Fisk, J. Sarrao, and J. Thompson, J. Solid State Chem. **158**, 25 (2001).
[17] A. C. Shockley, A. D. Dioguardi, N. apRoberts-Warren, P. Klavins, and N. J. Curro, J. Phys. Conf. Ser. **344**, 012020 (2011).
[18] C. P. Slichter, *Principles of Magnetic Resonance* (Springer, Berlin, 1990).
[19] Y.-f. Yang and D. Pines, Proc. Natl. Acad. Sci. USA **109**, E3060 (2012).
[20] M. Jiang, N. J. Curro, and R. T. Scalettar, Phys. Rev. B **90**, 241109(R) (2014).
[21] A. C. Shockley, N. apRoberts-Warren, D. M. Nisson, P. L. Kuhns, A. P. Reyes, S. Yuan, and N. J. Curro, Phys. Rev. B **88**, 075109 (2013).
[22] Y.-F. Yang and D. Pines, Phys. Rev. Lett. **100**, 096404 (2008).
[23] T. Ohama, H. Yasuoka, D. Mandrus, Z. Fisk, and J. L. Smith, J. Phys. Soc. Jpn. **64**, 2628 (1995).
[24] N. J. Curro, B. Simovic, P. C. Hammel, P. G. Pagliuso, J. L. Sarrao, J. D. Thompson, and G. B. Martins, Phys. Rev. B **64**, 180514(R) (2001).
[25] A. D. Christianson, E. D. Bauer, J. M. Lawrence, P. S. Riseborough, N. O. Moreno, P. G. Pagliuso, J. L. Sarrao, J. D. Thompson, E. A. Goremychkin, F. R. Trouw, M. P. Hehlen, and R. J. McQueeney, Phys. Rev. B **70**, 134505 (2004).
[26] T. Willers, Z. Hu, N. Hollmann, P. O. Körner, J. Gegner, T. Burnus, H. Fujiwara, A. Tanaka, D. Schmitz, H. H. Hsieh, H.-J. Lin, C. T. Chen, E. D. Bauer, J. L. Sarrao, E. Goremychkin, M. Koza, L. H. Tjeng, and A. Severing, Phys. Rev. B **81**, 195114 (2010).
[27] P. Monthoux, D. Pines, and G. G. Lonzarich, Nature (London) **450**, 1177 (2007).